

Hunt for the mHz variability in the TESS and *XMM-Newton* observations of nova-like cataclysmic variables

ANDREJ DOBROTKA,¹ JOZEF MAGDOLEN,¹ AND MARTIN MELICHERČÍK¹

¹*Advanced Technologies Research Institute, Faculty of Materials Science and Technology in Trnava, Slovak University of Technology in Bratislava, Bottova 25, 917 24 Trnava, Slovakia*

ABSTRACT

We analysed the flickering of selected nova-like cataclysmic variables observed by the TESS satellite and *XMM-Newton*. We searched for break frequencies (f_b) in the corresponding power density spectra (PDS), and for any long-term evolution. We found a new optical f_b in three nova-like systems and confirmed that the value of this frequency is clustered around 1 mHz. V504 Cen and V751 Cyg show possible X-ray counterparts of f_b that had previously only been seen in MV Lyr. This points towards the very central disc for source localisation. We investigated a previously proposed correlation between white dwarf mass and f_b , but thanks to the new measurements we do not conclude its existence. V3885 Sgr and V1193 Ori show flaring activity in the long-term light curve during which TESS observations were made. The corresponding PDSs show changes in shape and disappearance of f_b . TT Ari and SGRt 062340.2-265715 exhibit smooth changes in the long-term optical light curve, and the corresponding TESS observations show variable f_b during these changes. f_b is higher for lower brightness, which was seen only in MV Lyr so far.

Keywords: [Stellar accretion disks \(1579\)](#) — [Cataclysmic variable stars \(203\)](#) — [White dwarf stars \(1799\)](#)

1. INTRODUCTION

Nova-like systems are a subgroup of cataclysmic variables (CVs). These are interacting binaries powered by an accretion process. If the magnetic field of the central object is not strong enough, an accretion disc is present. The mass is transferred from a main sequence companion star via Roche lobe overflow, and flows towards the central white dwarf (WD) (see e.g. [B. Warner 1995](#) for a review).

CVs are either in high or low optical brightness states. These states depend on the mass accretion rate \dot{m}_{acc} through the disc. In the high state, \dot{m}_{acc} is high, the disc is bright and hot, and the hydrogen is fully ionised. When \dot{m}_{acc} decreases, the disc transitions to the low state, becoming cold, and the hydrogen recombines. The alternation between these two states is typical for dwarf novae and is driven by viscous-thermal instability ([Y. Osaki 1974](#); [R. Hōshi 1979](#); [F. Meyer & E. Meyer-Hofmeister 1981](#)). In the high state, the accretion disc is (almost) fully developed up to the WD, while it is truncated in the low state. This

truncation explains the delays between optical, UV radiation, and X-rays (see e.g. [M. R. Schreiber et al. 2003](#)).

Nova-likes are CVs with a high mass transfer from the secondary star. The \dot{m}_{acc} is sufficient to maintain the accretion disc in a quasi-permanent high state. This is because \dot{m}_{acc} is above a critical value, and the viscous-thermal instability does not appear. However, some fluctuations in mass transfer from the secondary, probably due to star spots, occasionally appear, and the nova-likes experience a sudden transition to a low state for a relatively short time ([R. K. Honeycutt & S. Kafka 2004](#)).

A typical manifestation of the underlying accretion process is fast stochastic variability, called flickering. The power density spectra (PDS) of this variability exhibit the shape of red noise or band limited noise, with characteristic frequencies in the form of a break f_b or Lorentzian ([S. Scaringi et al. 2012](#); [A. Dobrotka et al. 2016](#)). These characteristic frequencies provide information on the timescales of the physical processes that generate the variability. Thanks to new instruments such as the *Kepler* spacecraft, we know that the PDSs of CVs show a multi-component character. Well-studied cases are MV Lyr ([S. Scaringi et al. 2012](#)), V1504 Cyg ([A. Dobrotka & J.-U. Ness 2015](#)) and

V344 Lyr (A. Dobrotka et al. 2016). X-ray observations have also revealed multicomponent PDSs in systems such as SS Cyg (Ş. Balman & M. Revnivtsev 2012), RU Peg (A. Dobrotka et al. 2014) or MV Lyr (A. Dobrotka et al. 2017).

Kepler observations are ideal for the search for f_b . Thanks to the high quality data, it allows to track the evolution of this PDS parameter. A. Dobrotka et al. (2020) measured the time evolution of f_b during the transition of MV Lyr from high to low optical state and back. The authors concluded that f_b is rising towards the low state, and it returns to its original value after the system returns to the high optical state. This tells a lot about the behavior of the accretion disc, but unfortunately it is hard to say whether this behavior is typical for nova-likes in general, because there are no other measurements of this phenomenon.

S. Scaringi (2014) proposed a sandwich model to explain the presence of the $\log(f/\text{Hz}) \simeq -3$ signal detected in MV Lyr. This model consists of a standard geometrically thin and optically thick disc surrounded by a geometrically thick and optically thin disc in the central disc region. This inner thick disc or corona is hot and radiates in X-rays. Such a corona consists of evaporated gas from the underlying geometrically thin disc (F. Meyer & E. Meyer-Hofmeister 1994). The radiated X-rays are reprocessed into optical by the geometrically thin disc. The physical origin of the variability is explained by propagating mass accretion fluctuations (Y. E. Lyubarskii 1997; O. Kotov et al. 2001; P. Arévalo & P. Uttley 2006) occurring within the corona.

The X-ray origin of the variability was confirmed by *XMM-Newton* observations of the nova-like MV Lyr (A. Dobrotka et al. 2017), where the dominant frequency close to $\log(f/\text{Hz}) \simeq -3$ was also present in the X-rays. So far this is the only detection of a characteristic PDS frequency in optical and X-rays in a nova-like, showing consistent values and pointing towards a common physical origin. It supports the sandwich model interpretation, but it opens a question of whether such a correlation is present in nova-likes in general or if it is unique for MV Lyr.

Even if the sandwich model is known from X-ray binaries or AGNs (J. B. Dove et al. 1997), it has a serious energetic problem in CVs. The ratio of X-ray to optical luminosity in these binaries is of the order of 0.1 (see e.g. A. Dobrotka et al. 2020) or less (see e.g. Ş. Balman et al. 2014). Clearly, this is too low to explain the observed optical variability with the reprocessing scenario. A. Dobrotka et al. (2019) studied the flare profile of the flickering in the *Kepler* data of MV Lyr,

and found two components with different amplitudes. Both components, the central spike and the side-lobes, have similar characteristic frequencies of $\log(f/\text{Hz}) \simeq -3$, blending into the standard PDS and becoming indistinguishable. While the central spike is problematic to explain by the reprocessing due to too high amplitude, the low amplitude side-lobes match the scenario (A. Dobrotka et al. 2020). This suggests that the variability may originate in two separate regions.

A. Dobrotka et al. (2020) summarized various detections of f_b in the PDSs of CVs. The study implies that two characteristic frequencies can exist in the low state, while another frequency close to $\log(f/\text{Hz}) \simeq -3$ appears in the high state. This hunt for f_b continued in A. Dobrotka et al. (2024). 15 new f_b were detected among nova-like systems in a high optical state with apparent concentration of values between $\log(f/\text{Hz}) = -2.95$ and -2.84 . The probability that this signal close to 1 mHz is not a random feature of otherwise uniform distribution is at least 96%. Moreover, these f_b were detected in systems with low inclination. All PDSs with red noise without any f_b have considerably higher inclination. Finally, the authors also searched for correlation between the WD mass and f_b , but the low number of measurements did not allow a definite conclusion.

Apparently, the origin of the flickering variability in both the optical and X-rays is not well understood yet. The number of measured f_b in PDSs is still low, or even extremely low in X-rays. In this work, we focus on the search for f_b in PDSs calculated from TESS and *XMM-Newton* data of selected nova-like CVs. We focus on three different tasks; 1) to expand the number of measured f_b by A. Dobrotka et al. (2024), 2) to search for f_b correlation with optical state or its long-term behaviour, and 3) to search for f_b in X-rays.

In Section 2 we describe the selection of systems and the reduction of observations both from TESS and *XMM-Newton*. Sections 3 and 4 describe the PDS analysis of TESS and *XMM-Newton* data and their results, respectively. These results are discussed and summarized in Sections 5 and 6, respectively.

2. SELECTED SYSTEMS AND OBSERVATIONS

We first focused on TESS data of systems present in the Ritter's catalogue (H. Ritter & U. Kolb 2003) but not analysed in A. Dobrotka et al. (2024). The latter analysed nova-like systems studied in A. Bruch (2022), A. Bruch (2023a) and A. Bruch (2023b), where superhumps were detected. Superhumps together with the orbital period contaminates the PDS, therefore the known presence of these signals allowed us to define a suitable frequency interval of the PDS to be studied. In this

work, we selected SW Sex, UX UMa and VY Scl systems as subclasses of nova-likes (see B. Warner 1995 for review) in order to avoid undesired objects classified as nova-likes. We avoid, for example, intermediate polars with truncated discs and strong spin frequency, which can affect the PDSs (see Fig. 2 in A. Dobrotka et al. 2024). Intermediate polars and systems without disc, such as polars or compact binaries, such as AM CVn are also classified as nova-likes.

As a second step, we searched for *XMM-Newton* observations of all objects analysed in A. Dobrotka et al. (2024) and in this work.

As a third step, we selected *XMM-Newton* observations of objects with target type "CV" and "nova-like" in the *XMM-Newton* archive. However, these also include systems like magnetic polars without accretion disc, intermediate polars, AM CVn compact binaries with a hydrogen poor companion, or very old CVs known as period bouncers. We excluded them like in the TESS case and we focused on "standard" nova-like systems as studied in A. Dobrotka et al. (2024). We found observations of two systems not present in the TESS list from the previous step. SRGt 062340.2-265715 was simply not listed in the previous catalogue output, and V442 Oph does not have a TESS light curve.

For TESS light curves the Pre-search Data Conditioning Simple Aperture Photometry (PDCSAP) light curves were downloaded² from the Mikulski Archive for Space Telescopes (MAST) with a cadence of 120 seconds. The PDCSAP light curve is more suitable because systematic artifacts like long-term trends are removed.

For *XMM-Newton* light curves the data were downloaded from the XMM-Newton Science Archive (XSA), and we obtained light curves with the Science Analysis Software (SAS), version 21.0. We focused on the EPIC/pn detector due to its higher throughput. The light curves were extracted from a circular region with a radius of 20'' centred on the source, while the background was extracted from a region offset and the same radius. We used the `epproc` tool to re-generate calibrated events files, and `evselect` for light curve construction. We used a 50 s time bin. Since timing analysis is limited by the duration of the observation even if the source is very bright and the S/N ratio is very good, we excluded all observations shorter than 10 ks.

3. PDS ANALYSIS OF TESS DATA

For PDS calculation, we followed the same procedure as in A. Dobrotka et al. (2024). We selected light curves without large gaps empirically defined as a duration of

0.2 days or more. Within these light curves with no large gaps, we selected light curve portions with a duration of n_d days. Due to relatively large PDS scatter, we empirically derived the optimal value of $n_d = 10$. Not all of the examined objects have such uninterrupted 10 days intervals. Therefore, we redid the analysis also for $n_d = 5$. We could use the whole light curve portion between the gaps, but we prefer to have all PDSs equivalent with the same frequency resolution and PDS bin step.

To estimate the PDS, we divided each light curve portion into n_{subs} subsamples. For each subsample, we calculated a periodogram (power³ p as a function of frequency f) using the Lomb-Scargle algorithm⁴ (J. D. Scargle 1982). The whole f interval was rebinned with a constant frequency step of 0.1 dex, and all $\log(p)$ points within each frequency bin were averaged. Averaging of $\log(p)$, rather than p , is recommended by I. E. Papadakis & A. Lawrence (1993). A minimum number of averaged $\log(p)$ values per bin equal to $n_{\text{min}} \times n_{\text{subs}}$ (n_{min} points from each of n_{subs} periodograms per bin) must also be fulfilled. If the condition is not met, the bin should be broadened until the condition is fulfilled. This ensures enough points for calculating the mean value with the standard error of the mean.

The lowest PDS frequency (before re-binning) we took proportional to the duration of the light curve subsamples ($1/n_d$). Therefore, as n_{subs} and $n_{\text{min}} \times n_{\text{subs}}$ values, we chose 10 and 3×10 , respectively. The high-frequency end of the periodogram is set by the Nyquist frequency.

A. Dobrotka et al. (2024) focused on nova-like systems with known superhump periods, which are periods close to the orbital period. PDSs of such systems are contaminated by these signals, therefore the f_b search was limited to the interval from $\log(f/\text{Hz}) = -3.5$ to higher frequencies. Even though the systems selected in this work do not show superhumps, we kept the same studied frequency interval. It appears that PDSs of eclipsing systems are strongly contaminated by higher harmonics of the orbital period below $\log(f/\text{Hz}) = -3.5$.

Finally, we fitted the resulting PDSs with a broken power law model using the GNUPLLOT⁵ software.

3.1. Selection of positive detections

First, we selected only successful and credible fits. First criterion was that a broken power law fit must converge to f_b between $\log(f/\text{Hz}) = -3.5$ and -2.4 . If

³ We used power normalized by fractional rms.

⁴ We used python's package **Astropy** (Astropy Collaboration et al. 2013, 2018, 2022).

⁵ <http://www.gnuplot.info/>

² Using Python Lightcurve library; <https://docs.lightcurve.org>.

the PDS has a shape of a red noise, the broken power law is not able to do so, and f_b reached the lower end of the PDS. Second criterion was to have credible fits with acceptable uncertainty. We empirically selected 0.1 as an upper limit for f_b error. Larger errors resulted from too scattered PDS, and such f_b value is not credible. Therefore, all f_b with higher uncertainty than 0.1 were excluded.

After fitting all PDSs, and selecting successful and credible fits, we selected systems with positive detection of f_b . To ensure that the f_b is real, and is not just a random fluctuation of a scattered PDS, we consider a positive detection of f_b in a system when at least 50% ($n_p = 0.5$) of all PDSs yield a successful fit. This limit is based on the well-studied system MV Lyr, where we are certain from the *Kepler* data that f_b is present. TESS PDSs of the same object yield a successful fit with $n_p = 0.70$ and 0.77 for $n_d = 5$ and $n_d = 10$ (A. Dobrotka et al. 2024), respectively. Ideally, we would rely on the same n_p values, but MV Lyr is a much brighter system compared to many other selected nova-like, which makes detection easier. Therefore, a limit of $n_p = 0.5$ is a good compromise.

Finally, having only two light curve portions and $n_p = 0.5$ means that we have only one successful fit. This is not enough for a confident detection, therefore a minimal number of successful fits n_m we chose two.

Table 1 lists all selected nova-like observed by TESS. Clearly, almost all systems with no detection have n_p parameter 0 or very close to 0. Only two objects have values of 0.13 and 0.24 implying that few PDSs have successful fits. Nevertheless, this is too low and far from $n_p = 0.5$. Therefore, non-detection is practically unambiguous, and we found three systems with positive f_b detection.

3.2. Results

Applying $n_m = 2$ criterion, we got three positive detections; VY Scl, V3885 Sgr and SRGt 062340.2-265715. Case with $n_d = 10$ is only VY Scl. All corresponding PDSs with broken power law fits are depicted in Fig. 1. Individual f_b are shown as blue dots. The grey shaded area around these dots is the natural scatter of f_b due to noisy PDSs. This scatter is determined using the well-known MV Lyr case, and it represents the scatter of f_b calculated from TESS data (A. Dobrotka et al. 2024). Clearly, all blue points except the SRGt 062340.2-265715 case are within the scatter interval, therefore we do not expect any significant f_b variability between individual PDSs except SRGt 062340.2-265715.

All measured f_b values with starting times of the light curve portions are listed in Table 2. We compare also

Table 1. List of studied systems.

object	n_p	n_p	class
	$n_d = 10$	$n_d = 5$	
AH Pic	wn	wn	UX
BP Lyn	wn	wn	UX
CH CrB	–	low,wn	UX
CM Del	0	0	UX
HL Aqr	–	0	UX
HQ Mon	0	0	UX
HS 0139+0559	wn	wn	UX
HS 0220+0603	wn	wn	UX
HS 0229+8016	wn	wn	UX
HS 0455+8315	0	0	UX
HS 0642+5049	0	0.13	UX
HS 1813+6122	0.24	0.04	UX
IM Eri	wn	wn	UX
IX Vel	0	0.04	UX
OZ Dra	–	wn	UX
RW Sex	–	0	UX
SW Sex	0	0	UX
TT Tri	–	0	UX
V345 Pav	0	wn	UX
V363 Aur	0	0	UX
V1315 Aql	low	0	UX
V1776 Cyg	wn	wn	UX
V3885 Sgr	low	0.5	UX
WX Ari	0	0	UX
SRGt 062340.2-265715	no	0.8	UX
BO Cet	wn	wn	SW
EV Lyn	–	wn	SW
Leo 5	wn	wn	SW
V347 Pup	0	0	SW
V482 Cam	0	0	SW
GS Pav	–	wn	VY
LQ Peg	–	0	VY
TW Pic	0	0.02	VY
V380 Oph	–	low	VY
V794 Aql	–	low	VY
V1294 Tau	wn	wn	VY
VY Scl	1	0.5	VY
VZ Scl	–	0	VY

NOTE—The systems are listed by their class with UX, SW and VY meaning UX UMa, SW Sex and VY Scl, respectively. "low" means "low number" because the total number of light curve portions is one, and this is not able to fulfill the condition $n_m = 2$. "wn" means "white noise", and the corresponding PDS shows pure white noise or substantial part of the PDS including $\log(f/\text{Hz}) = -3$ is dominated by white noise (flat PDS without any slope). n_p parameter naturally equals zero.

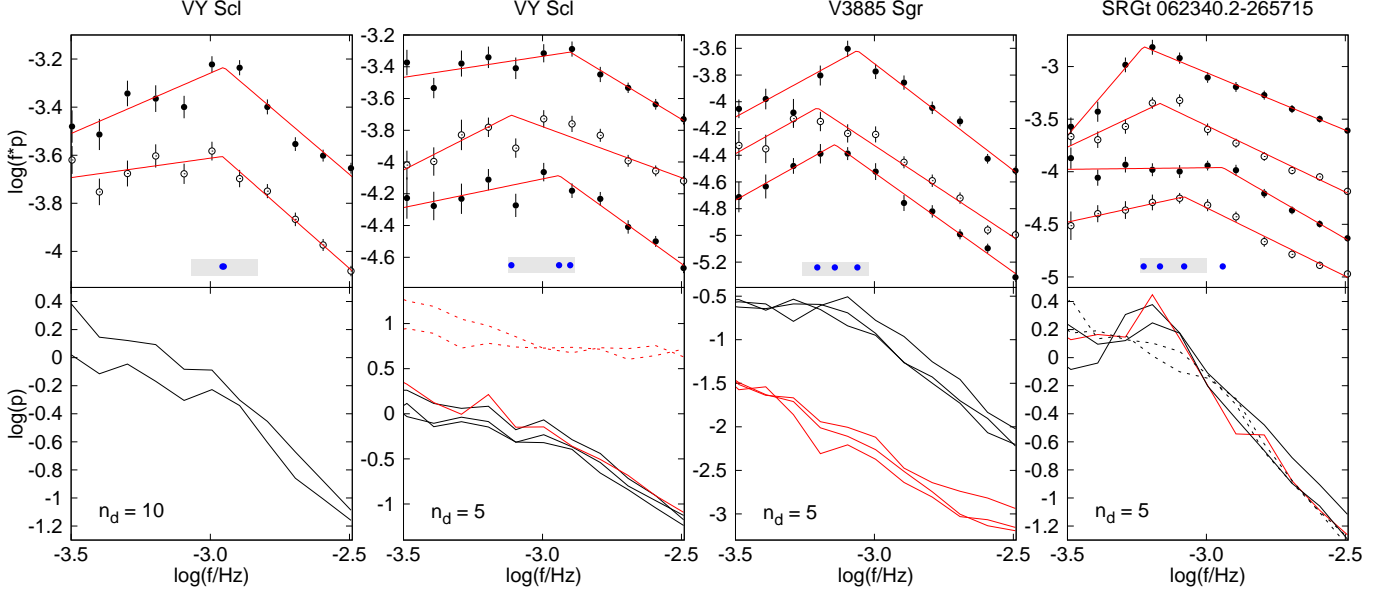


Figure 1. PDSs of three systems with positive detection of f_b . Upper panel - PDSs with positive detection of f_b for $n_d = 10$ and 5 light curves (points with errors of the mean). Red lines represent fits yielding f_b values with error lower than 0.1. PDSs are vertically offset for better visualisation. Individual f_b are shown as blue dots. The grey area around blue dots represents the natural scatter due to TESS light curve quality. The point style is varying just for clarity of the figure. Lower panel - all PDSs with (black lines) and without (red lines) positive detection of f_b . Dashed lines represent low(er) optical state.

χ^2_{red} for a broken power law fit yielding f_b with simple red noise. Clearly, the red noise fits are unambiguously excluded. Seven broken power law fits yield χ^2_{red} close to 1, while five are close to or higher than 1.5. The latter cases are natural for the limited performance of the TESS satellite and relatively scattered PDSs. Nevertheless, the broken power law fits are unambiguously better than simple red noise fits.

The weighted averages of f_b are summarized in Table 3. Since SRGt 062340.2-265715 has too scattered f_b measurements that imply variability, it must be taken with caution. The fitted $\log(f_b/\text{Hz})$ values are -3.23 ± 0.02 , -3.17 ± 0.03 , -2.94 ± 0.03 and -3.08 ± 0.03 . The first two values are consistent with the value of -3.2 , while the last two f_b are higher. If we take also another PDS not satisfying conditions for a successful fit⁶ it has a value of -3.19 ± 0.13 also consistent with -3.2 . Therefore, majority of fitted PDSs point toward $\log(f_b/\text{Hz}) = -3.2$, and we use the first two successful fits for the weighted average. The two measurements with higher f_b will be discussed later.

Distribution of all detected f_b together with those from A. Dobrotka et al. (2024) is depicted in the left panel of Fig. 2.

⁶ Because of error of 0.13 which is slightly larger than the predefine limit of 0.10.

4. PDS ANALYSIS OF *XMM-Newton* DATA

We used the same method for PDS estimate like for TESS data. The main difference is the duration of the observations. With *XMM-Newton* we don't have the luxury of selecting 5 or 10 days portions, and to divide these light curves into 10 subsamples. Typical duration of *XMM-Newton* observation is between 20 and 40 ks (based on the histogram of selected observations). This is 0.23 to 0.46 day, which is incomparable with TESS portions. Apparently, for *XMM-Newton* observation we must use different divisions. Moreover, for TESS case we have more such light curve portions, therefore we can define what is a positive detection. For *XMM-Newton* we must usually rely on a single observation.

For *XMM-Newton* PDS estimate we used $n_{\text{subs}} = 2$ and 3, and as a minimal number of points per bin we used 6 ($n_{\text{subs}} \times 2$ or 3). We searched for f_b using the same fit as for TESS data. Since orbital and superhump periods are not standardly seen in X-rays, we fitted the PDSs from $\log(f/\text{Hz}) = -4.0$ to -2.0 .

All PDSs calculated from *XMM-Newton* data are shown in Fig. 3. All ObsIDs of analysed observations and measured f_b values are listed in Table 4. We also quote the corresponding χ^2_{red} for the broken power law and a simple red noise model. The weighted averages of the candidates f_b are summarized and compared to the TESS detections (if any) in Table 3.

The first four PDSs in Fig. 3 do not show any structure indicating the presence of f_b . TW Pic has two observa-

Table 2. Selected f_b for systems with positive detection using $n_d = 10$ (first row, above the line), and $n_d = 5$ (below the line).

object	start (MJD)	$\log(f_b/\text{Hz})$	χ^2_{red} BPL/RN	start (MJD)	$\log(f_b/\text{Hz})$	χ^2_{red} BPL/RN
VY Scl	2088.245	-2.952(046)	2.57/13.79	2102.333	-2.956(039)	1.07/8.41
VY Scl	2088.245	-2.900(045)	0.78/5.59	2093.245	-3.112(094)	2.71/5.81
	2102.333	-2.940(043)	1.05/6.54			
V3885 Sgr	1658.373	-3.062(034)	1.71/17.74	1672.273	-3.206(057)	1.52/5.79
	1677.273	-3.142(024)	0.53/8.71			
SRGt 062340.2-265715	2206.737	-3.226(017)	0.48/14.71	2220.439	-3.167(033)	1.49/9.73
	3669.733	-2.941(032)	0.67/6.71	3683.695	-3.080(030)	0.74/6.11

NOTE—Start denotes the starting time of the selected light curve portion with MJD = JD - 2457000. The values in parenthesis represent the errors. For the χ^2_{red} we quote values for broken power law (BPL) and simple red noise (RN).**Table 3.** Weighted averages of measured f_b for individual systems with positive TESS detection (from this work and from A. Dobrotka et al. 2024 for direct comparison with *XMM-Newton* measurements) and from *XMM-Newton* observations.

object	$\log(f_b/\text{Hz})$ TESS	n_d	$\log(f_b/\text{Hz})$ <i>XMM-Newton</i>
VY Scl	-2.954 ± 0.030	10	—
	-2.940 ± 0.030	5	—
V3885 Sgr	-3.126 ± 0.019	5	—
SRGt 062340.2-265715	-3.213 ± 0.015	5	—
V504 Cen	-2.860 ± 0.046	10	-3.003 ± 0.332
V751 Cyg	-2.982 ± 0.023	10	-2.991 ± 0.134

NOTE—Below the line are two TESS measurements from A. Dobrotka et al. (2024).

white noise

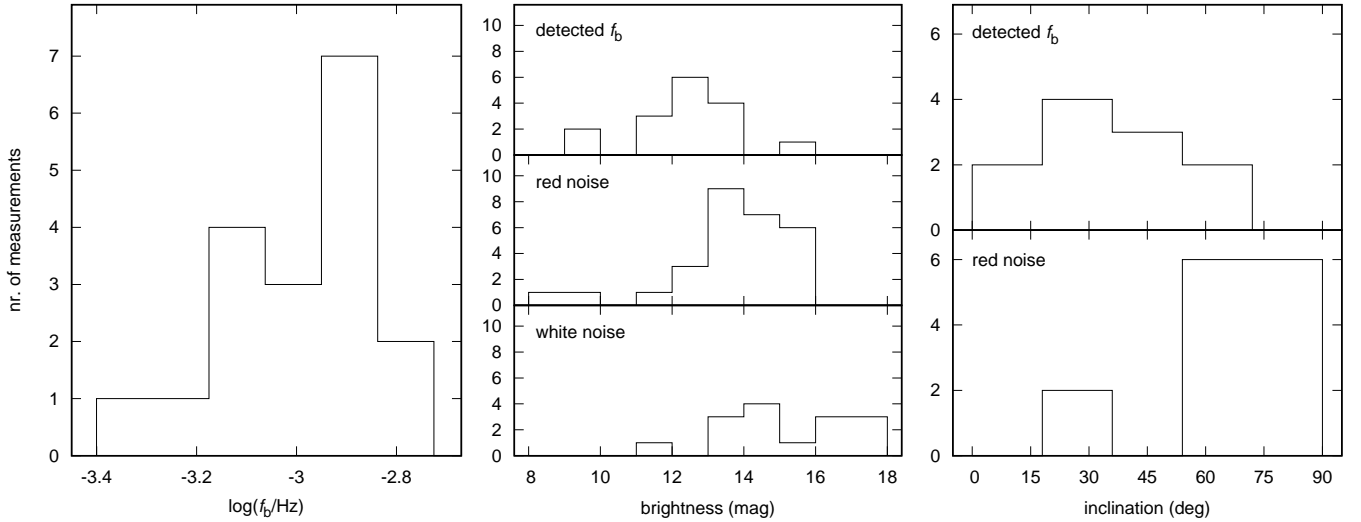
**Figure 2.** Number of nova-likes with detected and non-detected f_b for various parameters. The values are from this work and from A. Dobrotka et al. (2024). Left panel - number of detected f_b per frequency interval for nova-like CVs observed by TESS with condition $n_m \geq 2$. Middle panel - Number of systems per magnitude interval with detected and non-detected f_b . Right panel - Number of systems brighter than 14 mag per inclination interval with and without detection of f_b .

Table 4. Analysed *XMM-Newton* observations and measured f_b .

object	ObsID	$\log(f_b/\text{Hz})$	χ^2_{red}	$\log(f_b/\text{Hz})$	χ^2_{red}	duration (ks)
		$n_{\text{subs}} = 2$	BPL/RN	$n_{\text{subs}} = 3$	BPL/RN	
IX Vel	0111971001	—	—	—	—	19.0
TW Pic	0500970101	—	—	—	—	41.4
	0500970301	—	—	—	—	16.0
UU Aqr	0930800101	—	—	—	—	17.4
V442 Oph	0305440801	—	—	—	—	11.5
SRGt 062340.2-265715	0901220101	-2.984 ± 0.118	2.61/5.18	-3.008 ± 0.140	1.87/4.66	44.1
		-2.347 ± 0.060	2.09/4.83	-2.445 ± 0.085	2.05/4.33	
V1084 Her	0804110101	-3.051 ± 0.191	1.37/1.48	-2.976 ± 0.300	1.38/1.43	21.0
UX UMa	0084190201	—	—	-3.155 ± 0.104	0.57/0.80	45.9
		—	—	-3.120 ± 0.203	0.64/0.81	
V504 Cen	0311590401	—	—	-3.003 ± 0.332	0.75/3.76	19.9
V751 Cyg	0679580201	-3.064 ± 0.226	1.57/2.54	-2.952 ± 0.166	0.96/2.12	25.6

NOTE—Duration is the duration of the EPIC/pn light curve. If two values are quoted for one ObsID, the first is for fitting interval from $\log(f/\text{Hz}) = -4.0$, and the second is from $\log(f/\text{Hz}) = -4.5$. For the χ^2_{red} we quote values for broken power law (BPL) and simple red noise (RN).

tions. Since both have the same characteristics, we show only the longer-one. All PDSs from the four nova-like are consistent with a red noise shape, only the V442 Oph case is too short (11.5 ks) to confirm the pure red noise nature of the PDS. Otherwise, the non-detection of any f_b in these systems is consistent with conclusions from the TESS data.

Some deviations from simple red noise are possible for SRGt 062340.2-265715. The χ^2_{red} are much better for broken power laws, but the values are still too large. For consistency check we fitted the PDS also from $\log(f/\text{Hz}) = -4.5$, and the resulting f_b is different. Apparently, the PDS does not show any robust trend, and we conclude no detection for this object. Another PDS with possible f_b is seen in V1084 Her. However, χ^2_{red} are practically the same for the broken power law model and red noise. Therefore, we conclude no detection in this case too. UX UMa shows very scattered PDS with $n_{\text{subs}} = 2$ but a changing red noise slope is seen for $n_{\text{subs}} = 3$. Fit with lower PDS end of $\log(f/\text{Hz}) = -4.5$ yields consistent f_b value with the original fit. However, even if the χ^2_{red} from the broken power law are lower than in the red noise case, the difference is small and lower than one. This suggests overfitting due to large PDS errors. No conclusion can be derived, and we conclude no detection. The non-detections of f_b in V 1084 Her and UX UMa agree with the non-detections in TESS data.

The last two examples represent potential detections of f_b . Deviations from a simple red noise are noticeable for V504 Cen. The $n_{\text{subs}} = 2$ case shows a possible change of the red noise trend at approximately $\log(f/\text{Hz}) = -3.31$, but the different slope towards the lower frequencies is represented by only one single point. This is insufficient for any fitting. The changing slope is better seen and represented by more PDS points in the $n_{\text{subs}} = 3$ case. Due to the complicated PDS shape toward higher frequencies we used three linear functions and changed the higher frequency end for fitting to $\log(f/\text{Hz}) = -2.2$. Differences in χ^2_{red} clearly support the broken power law model. The fitted f_b has relatively large error but the value of $\log(f_b/\text{Hz}) = -3.00 \pm 0.33$ agrees with the TESS detection in A. Dobrotka et al. (2024). Finally, both $n_{\text{subs}} = 2$ and 3 of V751 Cyg show a clear change of the red noise slope close to $\log(f/\text{Hz}) = -3$. χ^2_{red} supports broken power law as a better model mainly for $n_{\text{subs}} = 3$. The averaged value of $\log(f_b/\text{Hz}) = -2.99 \pm 0.13$ agrees with the TESS detection in A. Dobrotka et al. (2024).

5. DISCUSSION

We searched for f_b of the flickering of nova-like CVs in optical and X-ray data from TESS and *XMM-Newton*

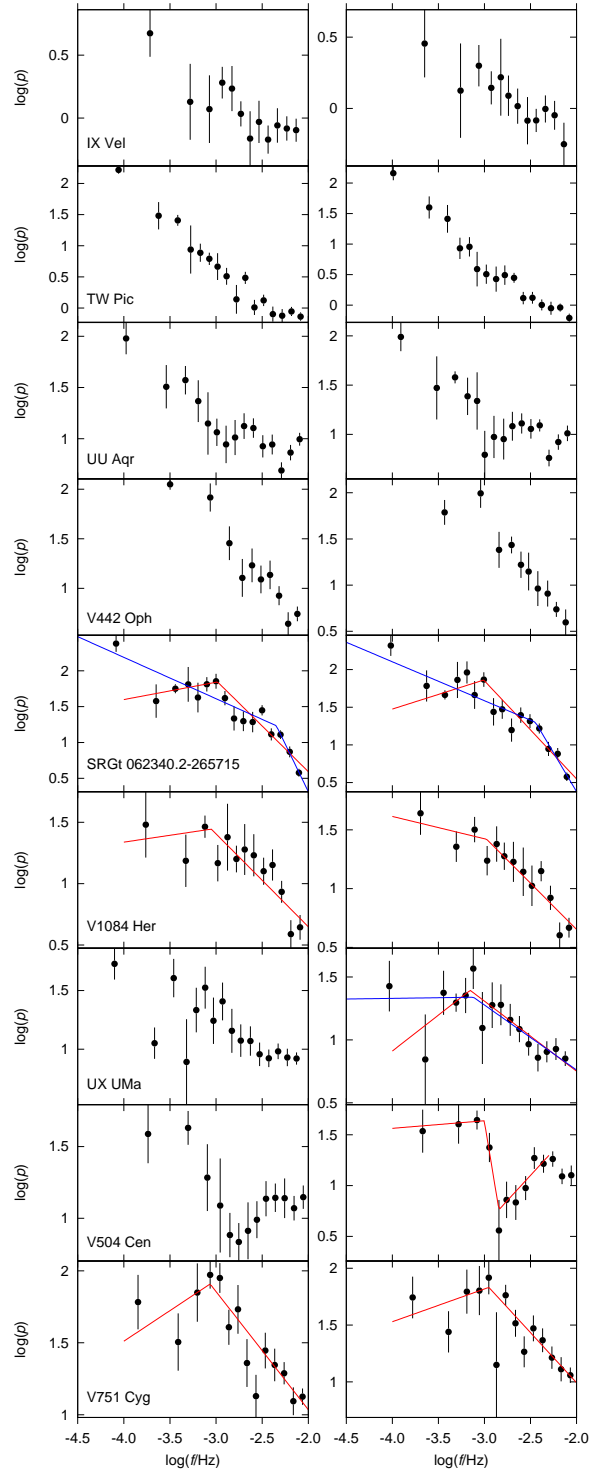


Figure 3. PDSs calculated from *XMM-Newton* observations using $n_{\text{subs}} = 2$ (left column) and 3 (right column). Red lines are the fits to the PDSs with lower PDS end of $\log(f/\text{Hz}) = -4.0$ while blue is from $\log(f/\text{Hz}) = -4.5$.

respectively. We found three new f_b in optical and two new f_b in X-rays. The latter agrees with previously detected optical values.

5.1. PDS break frequency detection

A. Dobrotka et al. (2020) found a possibility that CVs in a high state show a preferred characteristic PDS frequency close to $\log(f/\text{Hz}) = -3$. The authors summarized f_b measurements of five systems, with only three showing values close to $\log(f/\text{Hz}) = -3$. One is the nova-like MV Lyr, and the two remaining are dwarf novae V1504 Cyg and V344 Lyr. Apparently, the number of studied systems was low, therefore, it is still possible that the weak peak in the corresponding histogram is a random result of an otherwise uniform distribution. The authors simulated such histograms and found that the probability⁷ that the peak is not random is only 69%.

The systematic search for f_b in selected nova-like CVs using TESS data performed by A. Dobrotka et al. (2024) yields a much larger data sample than in A. Dobrotka et al. (2020). In addition to the known MV Lyr, the authors found 14 other new detections. The resulting distribution of f_b shows a concentration of values between $\log(f/\text{Hz}) = -2.95$ and -2.84 with a probability of 99% not being a result of a random process. This probability is for the same criterion ($n_m = 2$) as used in this work. The three new measurements from this work slightly increase the number of detected f_b , but not in the potentially preferred interval between $\log(f/\text{Hz}) = -2.95$ and -2.84 . The confidence of 99% decreases to 96.6%. Clearly, based on Fig. 2 the f_b distribution is continuous and not structured into several values like discussed by A. Dobrotka et al. (2020). The potentially preferred value is probably just a maximum of the distribution.

f_b derived from *XMM-Newton* observations have larger errors compared to the TESS results. This is due to a very short observation duration which is typical for *XMM-Newton*. The main result of this analysis is that optical f_b have a possible X-ray counterpart in V504 Cen and V751 Cyg. So far this was demonstrated only for MV Lyr by A. Dobrotka et al. (2017).

5.2. Break frequency vs long-term light curve

If a system exhibits f_b , not all PDSs yield its detection. This is due to the natural scatter of PDS points. Usually, such PDSs do not show any significant shape differences. However, A. Dobrotka et al. (2020) showed that PDS exhibits a change in its morphology, and f_b

can disappear during the transition from high to low optical state and vice versa. Therefore, non-detection of f_b can have a real physical reason. Instead of relying only on f_b detection or non-detection, we discuss also the shape of the PDS.

All three nova-likes with newly detected f_b show variability of PDS morphology. The shape and normalised power levels differ for PDSs with and without detection of f_b in VY Scl and V3885 Sgr. In VY Scl two groups of PDSs are seen. The red dashed lines in Fig. 1 show a simple white noise implying absence of any flickering with typical red noise. As shown in the ASAS-SN light curve in Fig. 4, the corresponding observations were taken during the low state where the object is very faint and TESS is not able to detect any variability. Otherwise, this would be an excellent opportunity to study f_b difference between high and low optical state. One PDS without f_b detection is also taken during the high state (red solid line), but this is only because of error 0.11, which is slightly above the criterion we used for a successful fit.

V3885 Sgr shows a different behaviour. The PDS power is considerably lower when PDS has a clear red noise shape without any f_b detection. Long-term ASAS-SN light curve in Fig. 4 shows flaring activity and individual TESS observations are taken during different stages of this flaring. f_b is detected during a temporarily higher state seen as a local rebrightening at approximately $\text{JD} - 2450000 = 8650$. All other TESS observations outside of this rebrightening show simple red noise. This suggests a real change in flickering characteristics. Similar flaring variability has been observed in VY Scl systems when the disc is in the high state, for example in V794 Aql (R. K. Honeycutt et al. 1994, R. K. Honeycutt & J. W. Robertson 1998), FY Per (R. K. Honeycutt 2001) or V4743 Sgr (A. Dobrotka et al. 2021). Either the flares are due to disc instabilities when mass transfer from the secondary temporarily ceases (R. K. Honeycutt et al. 1994), or the disc remains in the high state while the variability is caused by mass transfer variations from the secondary (R. K. Honeycutt & J. W. Robertson 1998). Varying mass transfer naturally generates changes in the accretion disc flow. This variable flow affects the structure of the disc, which is seen as changes or disappearance of f_b .

Finally, as already mentioned, we see a drift of f_b for SRGt 062340.2-265715. The f_b values are -3.23, -3.17, -2.94, and -3.08. The first observations with $\log(f_b/\text{Hz})$ equal to -3.23, -3.17 (one additional red line at -3.19) are taken during a high state (upper panel of Fig. 4). A transition occurs approximately at $\text{JD} - 2450000 =$

⁷ Based on number of simulated histograms with the same or higher peaks as the observed histogram.

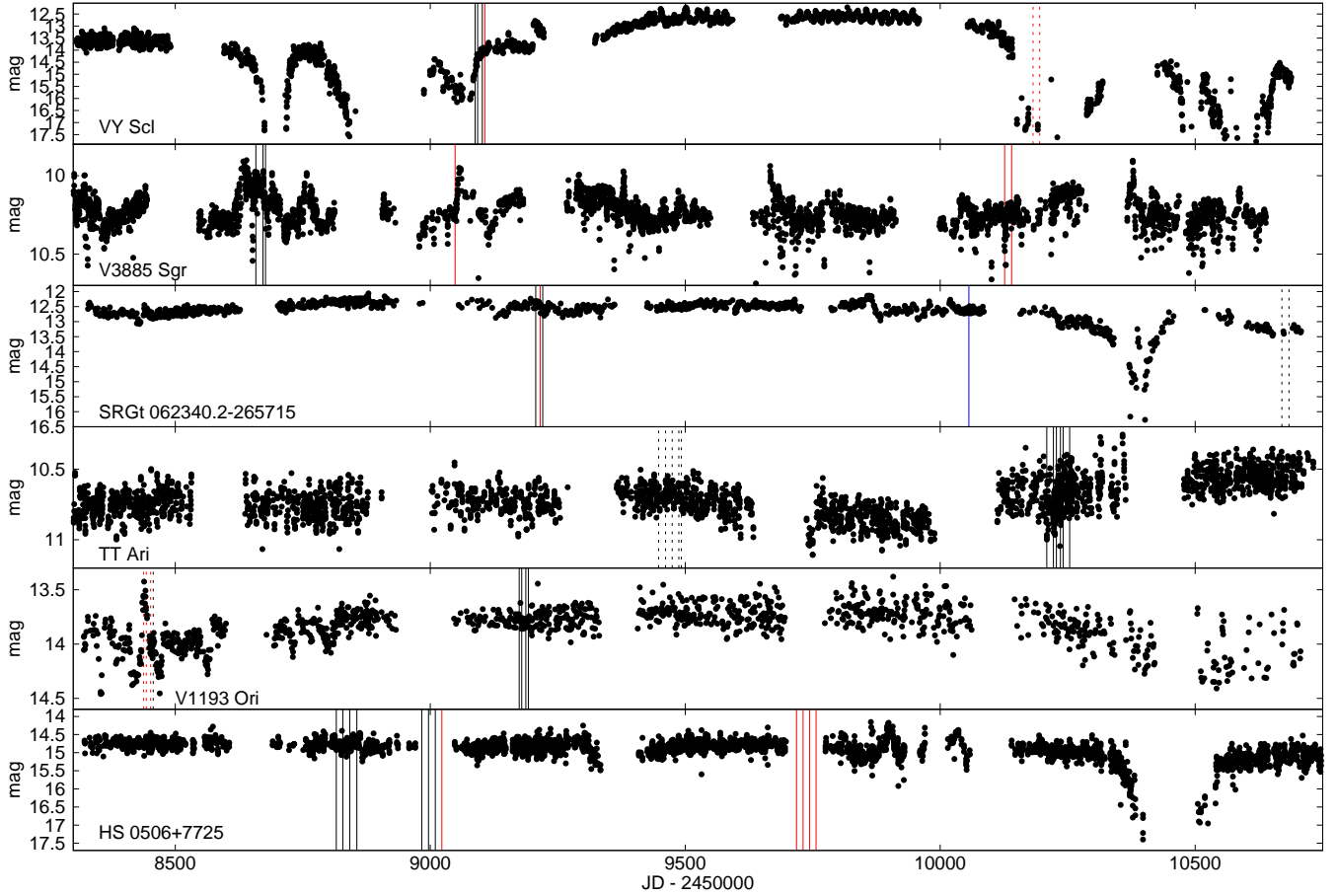


Figure 4. ASAS-SN light curves of selected systems with detected f_b . Vertical lines represent time of TESS light curve portions with detected (black lines) and non-detected (red lines) f_b . Blue vertical line shows the time of *XMM-Newton* observation. Dashed lines represent observations taken during specific times discussed in the text (corresponding to dashed PDSs in Fig. 1 and 5).

10400, the system returns back to the high state, and another transition starts subsequently. Two TESS observations yielding $\log(f_b/\text{Hz})$ of -2.94 and -3.08 are taken during this second transition (dashed lines in Fig. 4). A. Dobrotka et al. (2020) showed that during the transition of MV Lyr to the low state the f_b rises. Therefore, SRGt 062340.2-265715 is a second case where such rising f_b during a transition to the low state was observed.

A. Dobrotka et al. (2024) did not study such PDS morphology, and focused only on f_b detection. The authors took into account the long-term light curve only if f_b showed an anomalous value. Therefore, we redid the PDS calculation of the objects the authors studied, and we searched for any systematic PDS shape change like found in this work. We found three systems with such behavior; TT Ari, V1193 Ori and HS 0506+7725.

PDSs of TT Ari and its ASAS-SN light curve are shown in Figs. 5 and 4, respectively. The long-term light curve does not show any flaring like in V3885 Sgr, nor the transition typical for VY Scl, but a noticeable

difference in brightness level and amplitude of variability during the TESS observations is seen instead. Clear are two "groups" of PDSs. Lower PDS power is seen before JD - 2450000 = 9500. Subsequently, the brightness slightly decreases and after JD - 2450000 = 10000 it increases back or even to a slightly higher brightness level. TESS observations taken during this second stage show higher power suggesting a higher amplitude of variability. This higher amplitude is seen as considerably higher data scatter during the second group of TESS observations. Based on A. Dobrotka et al. (2024) the brighter stage (later observations) yields lower values of f_b . This behaviour is in agreement with the conclusion from A. Dobrotka et al. (2020) where f_b showed lower values for a higher optical state. Apparently, the accretion exhibits some fluctuation after JD - 2450000 = 9500, and affects the PDS power with f_b value.

V1193 Ori PDSs in Fig. 5 shows three PDSs slightly offset towards lower power. This is clear mainly for higher frequencies where f_b is located. The PDS power

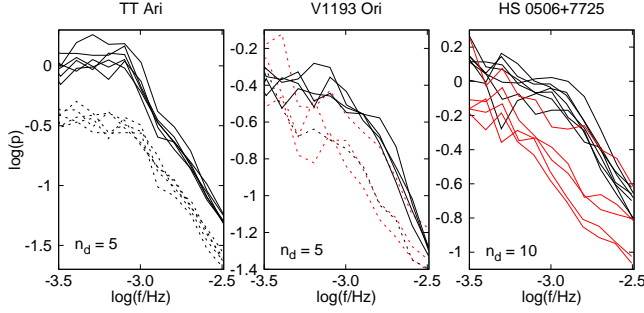


Figure 5. PDSs of TT Ari, V1193 Ori and HS 0506+7725. Black lines represent PDSs with f_b detection, and red lines without. Dashed lines represent PDSs taken during specific times shown as dashed lines in Fig. 4 (see text for details).

at low frequencies is more or less similar. This is very similar to the PDS change during state transitions in MV Lyr (A. Dobrotka et al. 2020). ASAS-SN light curve (Fig. 4) shows one flare during which the PDS did not yield f_b detection. Once the brightness level is stabilized, the PDSs yield detection of f_b . The dashed lines in Fig. 5 depict the PDSs taken during or close to the flare at approximately JD - 2450000 = 8400. No clear correlation between optical states is seen, but flaring activity indicates a sort of instability during which the accretion disc experiences changes. Then the PDS is affected and f_b is modified or even disappears.

The final and most challenging case is HS 0506+7725. The PDSs in Fig. 5 show a similar behaviour as in the V 1193 Ori case. The f_b disappeared or decreased in power while the low frequency parts of all PDSs are more or less comparable. However, no state transition is seen in the long-term light curve (Fig. 4). Any statement about state transition is still not conclusive because eight observations were taken during gaps and we don't see how the brightness evolved. We cannot rule out any flaring activity during the four red PDSs seen in Fig. 5.

Finally, we conclude that variable optical brightness generates PDS change and f_b modification or even disappearance. Such variable brightness or flaring indicates fluctuations in mass transfer rate, and significant changes in the accretion flow are a consequence. Naturally, f_b as a finger-print of the accretion flow must answer. If f_b variability is detected, its value increases with decreasing brightness, as concluded by A. Dobrotka et al. (2020). Apparently, this behaviour is not typical only for MV Lyr but probably for more or all nova-likes. This suggests a common physical origin of the fast variability in these objects.

5.3. Dependence on system parameters

A. Dobrotka et al. (2024) compared WD masses m_{WD} to detected f_b values. They proposed a possibility that

Table 5. System parameters of selected systems.

object	incl. (deg)	m_{WD} (M_\odot)
VY Scl	30 ^(a)	1.22 ± 0.22 ^(a)
V3885 Sgr	45-75 ^(b)	0.70 ^(c)
CM Del	73 ^(a)	
HL Aqr	19 - 27 ^(e)	
IX Vel	57 ^(a)	
RW Sex	34 ^(a)	
SW Sex	ecl	
TT Tri	ecl	
TW Pic	<40 ^(f)	
VZ Scl	ecl	
WX Ari	ecl	
V345 Pav	ecl	
V347 Pup	ecl	
V363 Aur	ecl	
V380 Oph	42 ^(a)	
V482 Cam	ecl	
V794 Aql	60 ^(g)	
V1315 Aql	ecl	

NOTE—First part is for systems with f_b detection, while second part is only for systems with red noise PDSs. Eclipsing (ecl) systems were identified in this work based on the morphology of the light curve.

- ^(a)H. Ritter & U. Kolb (2003),
^(b)F. M. A. Ribeiro & M. P. Diaz (2007),
^(c)A. P. Linnell et al. (2009), ^(d)A. Aungwerojwit et al. (2005), ^(e)P. Rodríguez-Gil et al. (2007),
^(f)D. A. H. Buckley & I. R. Tuohy (1990),
^(g)P. Godon et al. (2007)

these two parameters are correlated. However, the number of measured f_b was low, but mainly the scatter and uncertainties of m_{WD} are high. After adding VY Scl and V3885 Sgr with m_{WD} from Table 5, we see no such correlation (Fig. 6).

Another possible correlation is detection of f_b and the inclination of the binary. A. Dobrotka et al. (2024) found that systems with detected f_b have lower inclination than 60-75°. Table 5 lists the inclinations of the systems studied in this work. Apparently, the systems with detected f_b confirm the conclusion of A. Dobrotka et al. (2024) that low inclination is required for f_b detection. However, the second part of the table already discredits the original hypothesis that non-detection of f_b is due to high inclination, where the central disc as a source of the flickering is hidden by the disc edge. We found that five systems do have lower inclination than 60° and do not show any f_b .

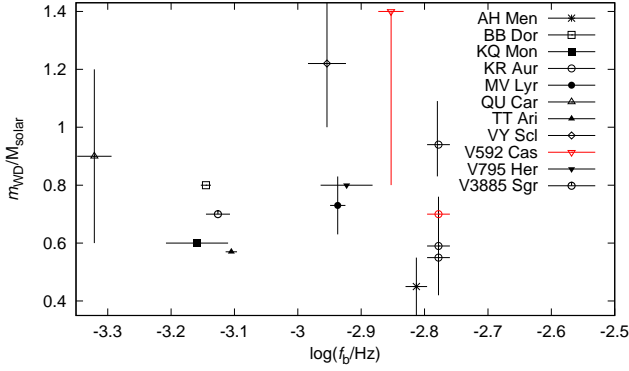


Figure 6. m_{WD} vs f_b from A. Dobrotka et al. (2024) together with VY Scl and V3885 Sgr studied in this paper. The red color represents uncertain measurements (see A. Dobrotka et al. 2024 for details).

A possible explanation can be simply based on limiting capabilities of TESS. MV Lyr is a well-studied system with clear f_b and it does not show it in all TESS light curve portions (A. Dobrotka et al. 2024). It is present only in 70% or 77% cases for $n_d = 5$ and $n_d = 10$, respectively. For example, TWPic PDS shows a weak bend or hump close to $\log(f/\text{Hz}) = -2.95$. Fitting the PDSs from $\log(f/\text{Hz}) = -3.35$, we found five similar PDSs yielding consistent f_b between $\log(f/\text{Hz}) = -2.9$ and -3.1 . Some have errors larger and some lower than 0.1. These features may be a weak manifestation of the presence of f_b . Apparently, a stronger instrument and more detailed PDS is needed.

Therefore, it is possible that in faint systems f_b is simply not detected. High inclination CVs tend to be fainter which could explain why f_b is not detected for these inclinations. In the middle panel of Fig. 2 we compare histograms of nova-likes per magnitude interval for three classes of objects⁸. The brightness span for systems with detected f_b is from 9.5 to 15.1 mag. Taking all systems showing only red noise the brightness span is from 9.0 to 15.7 mag, therefore very similar. Contrary, taking systems dominated by white noise the brightness span is offset to higher values from 11.1 to 18.0 mag. Apparently, there is no significant difference in brightness span for objects with f_b and red noise, but the bulk of distribution for red noise systems is offset toward lower magnitudes. This suggests that the brightness is not decisive, but probably plays an important role, and the non-detection of f_b is strongly biased by TESS capabilities.

⁸ We used magnitudes from H. Ritter & U. Kolb (2003) for objects from Table 1 of this work and Table 2 from A. Dobrotka et al. (2024).

Taking into account the brightness conclusion, we can set a limiting magnitude for histogram construction in the right panel of Fig. 2⁹. Taking 14 mag as the limit, where the majority of the distribution of systems with detected f_b ends, there are HL Aqr and RW Sex with low inclination showing red noise. The case for red noise systems is not conclusive, but it appears that systems with detected f_b are not high inclination binaries.

5.4. Physical origin of the break frequency

Based on this work and A. Dobrotka et al. (2017) we can conclude that three nova-likes show the same f_b in optical and X-rays. This suggests a common physical origin of the fast variability in these objects. The X-ray nature points toward the central corona or the boundary layer between the inner disc and the WD as the source of the variability. In the case of the corona, it supports the sandwich model proposed for MV Lyr by S. Scaringi (2014). However, additional information is needed to discriminate between the two scenarios.

A boundary layer could be connected to the inner disc radii. During the transition to a low state, the mass accretion drops, the inner disc starts to be truncated and the inner radius of the optically thick disc increases like in dwarf novae (see e.g. J.-P. Lasota 2001 for a review). The Kepler frequency as a potential counterpart of f_b should then decrease. The opposite was observed in MV Lyr (A. Dobrotka et al. 2020), and in SRGt 062340.2-265715 in this work. This rules out the inner disc radii as the source.

The central sandwich corona is a result of evaporation (F. Meyer & E. Meyer-Hofmeister 1994). If the mass accretion rate drops during the transition to the low state, also the evaporation of matter to the corona can drop. Such corona can shrink radially with increasing characteristic frequency as a result (top panel of Fig. 3 in S. Scaringi 2014). Such radial "shrinking" of the corona was observed in AGNs IRAS 13224-3809 (E. Kara et al. 2013) and 1H 0707-495 (D. R. Wilkins et al. 2014). The authors conclude that the X-ray source is more compact during low flux states.

Sandwich model is an attractive solution, but the energetic problem due to X-ray to optical luminosity ratio being lower than one (see e.g. Ş. Balman et al. 2014; A. Dobrotka et al. 2020) disqualifies the reprocessing scenario in which the optical radiation is generated by reprocessing of X-rays. The sandwich can still exist,

⁹ If the inclination is uncertain in an interval we used the averaged value. If the inclination has an upper limit, we used the upper limit. For systems with detected f_b , we did not apply the brightness filter.

but the optical radiation must be generated by the geometrically thin disc itself, and the same f_b in optical and X-rays implies common mass accretion fluctuations. Since the central corona is a result of evaporation of the thin disc (F. Meyer & E. Meyer-Hofmeister 1994), any fluctuation in this disc must result in fluctuations in evaporated matter. The common origin is natural then. Another possibility for the corona to play a role in X-ray flickering generation is based on a process known from AGNs. The soft disc photon from a geometrically thin disc irradiates the corona, and the photons are up-scattered to observed X-rays by the inverse Compton process (see e.g. F. Haardt & L. Maraschi 1991, 1993). If any mass accretion fluctuations characterised by f_b are present in the corona, this can leave imprints in the upscattered X-ray radiation.

6. SUMMARY AND CONCLUSIONS

We studied optical and X-ray flickering in selected nova-like cataclysmic variables observed by the TESS and *XMM-Newton* spacecrafts. We searched for f_b in the corresponding PDSs.

We found a new optical f_b in three systems, and confirmed the previously reported result (A. Dobrotka et al. 2024) that the value of f_b in nova-likes is clustered around 1 mHz. The long-term ASAS-SN light curves suggest that the PDS and f_b can vary in shape and in value during brightness changes. f_b can even disappear. If f_b is changing it follows the correlation found by A. Dobrotka et al. (2020), where f_b increases with decreasing brightness. A. Dobrotka et al. (2024) proposed that systems with detected f_b have lower inclination than approximately 60-75°, and that a correlation between WD mass and f_b may exist. Thanks to the new measurements in this work, we see no correlation with WD mass, but the inclination condition is confirmed. However, since higher inclination systems tend to be fainter, the non-detection can be a result of limited TESS capabilities. Therefore, the case with systems showing only red noise is not conclusive,

but it appears that nova-likes showing f_b are not high inclination systems. Exclusive of low brightness, the non-detection of f_b for higher inclinations can suggest obscuration of the flickering source being the central disc by the disc edge.

We found two new X-ray counterparts of optical f_b in V504 Cen and V751 Cyg. The presence of the same f_b in optical and X-rays was seen only in MV Lyr so far. This implies a similar physical origin of the flickering in more or all nova-likes in general, and points toward a very central disc for source localisation. The X-ray nature of the variability, together with the increasing value of f_b with decreasing optical brightness, supports the central sandwich corona as a potential source.

ACKNOWLEDGMENTS

Funded by the EU NextGenerationEU through the Recovery and Resilience Plan for Slovakia under the project No. 09I03-03-V04-00378. This work makes use of ASAS-SN data (B. Shappee et al. 2014; C. S. Kochanek et al. 2017). We thank anonymous referee for helpful report and for useful suggestions mainly in the case of inclination vs detection discussion.

AUTHOR CONTRIBUTIONS

AD came up with the initial research concept, analysed *XMM-Newton* data and wrote the manuscript. JM provided TESS data analysis and edited the manuscript. MM participated in data handling, figure preparation, and edited the manuscript.

Facilities: TESS, *XMM-Newton*

Software: astropy (Astropy Collaboration et al. 2013, 2018, 2022), GNUPLLOT (<http://www.gnuplot.info/>), SAS (<https://www.cosmos.esa.int/web/xmm-newton/sas>)

REFERENCES

- Arévalo, P., & Uttley, P. 2006, MNRAS, 367, 801, doi: [10.1111/j.1365-2966.2006.09989.x](https://doi.org/10.1111/j.1365-2966.2006.09989.x)
- Astropy Collaboration, Robitaille, T. P., Tollerud, E. J., et al. 2013, A&A, 558, A33, doi: [10.1051/0004-6361/201322068](https://doi.org/10.1051/0004-6361/201322068)
- Astropy Collaboration, Price-Whelan, A. M., Sipőcz, B. M., et al. 2018, AJ, 156, 123, doi: [10.3847/1538-3881/aabc4f](https://doi.org/10.3847/1538-3881/aabc4f)
- Astropy Collaboration, Price-Whelan, A. M., Lim, P. L., et al. 2022, ApJ, 935, 167, doi: [10.3847/1538-4357/ac7c74](https://doi.org/10.3847/1538-4357/ac7c74)
- Aungwerojwit, A., Gänsicke, B. T., Rodríguez-Gil, P., et al. 2005, A&A, 443, 995, doi: [10.1051/0004-6361:20042610](https://doi.org/10.1051/0004-6361:20042610)
- Balman, Ş., Godon, P., & Sion, E. M. 2014, ApJ, 794, 84, doi: [10.1088/0004-637X/794/1/84](https://doi.org/10.1088/0004-637X/794/1/84)
- Balman, Ş., & Revnivtsev, M. 2012, A&A, 546, A112, doi: [10.1051/0004-6361/201219469](https://doi.org/10.1051/0004-6361/201219469)
- Bruch, A. 2022, MNRAS, 514, 4718, doi: [10.1093/mnras/stac1650](https://doi.org/10.1093/mnras/stac1650)

- Bruch, A. 2023a, MNRAS, 519, 352,
doi: [10.1093/mnras/stac3493](https://doi.org/10.1093/mnras/stac3493)
- Bruch, A. 2023b, MNRAS, 525, 1953,
doi: [10.1093/mnras/stad2089](https://doi.org/10.1093/mnras/stad2089)
- Buckley, D. A. H., & Tuohy, I. R. 1990, ApJ, 349, 296,
doi: [10.1086/168314](https://doi.org/10.1086/168314)
- Dobrotka, A., Magdolen, J., & Janíková, D. 2024, A&A, 692, A27, doi: [10.1051/0004-6361/202451004](https://doi.org/10.1051/0004-6361/202451004)
- Dobrotka, A., Mineshige, S., & Ness, J.-U. 2014, MNRAS, 438, 1714, doi: [10.1093/mnras/stt2311](https://doi.org/10.1093/mnras/stt2311)
- Dobrotka, A., Negoro, H., & Konopka, P. 2020, A&A, 641, A55, doi: [10.1051/0004-6361/201935569](https://doi.org/10.1051/0004-6361/201935569)
- Dobrotka, A., Negoro, H., & Mineshige, S. 2019, A&A, 631, A134, doi: [10.1051/0004-6361/201935198](https://doi.org/10.1051/0004-6361/201935198)
- Dobrotka, A., & Ness, J.-U. 2015, MNRAS, 451, 2851,
doi: [10.1093/mnras/stv1178](https://doi.org/10.1093/mnras/stv1178)
- Dobrotka, A., Ness, J.-U., & Bajčičáková, I. 2016, MNRAS, 460, 458, doi: [10.1093/mnras/stw1001](https://doi.org/10.1093/mnras/stw1001)
- Dobrotka, A., Ness, J.-U., Mineshige, S., & Nucita, A. A. 2017, MNRAS, 468, 1183, doi: [10.1093/mnras/stx513](https://doi.org/10.1093/mnras/stx513)
- Dobrotka, A., Orio, M., Benka, D., & Vanderburg, A. 2021, A&A, 649, A67, doi: [10.1051/0004-6361/202039742](https://doi.org/10.1051/0004-6361/202039742)
- Dove, J. B., Wilms, J., Maisack, M., & Begelman, M. C. 1997, ApJ, 487, 759, doi: [10.1086/304647](https://doi.org/10.1086/304647)
- Godon, P., Sion, E. M., Barrett, P., & Szkody, P. 2007, ApJ, 656, 1092, doi: [10.1086/510775](https://doi.org/10.1086/510775)
- Hōshi, R. 1979, Progress of Theoretical Physics, 61, 1307,
doi: [10.1143/PTP.61.1307](https://doi.org/10.1143/PTP.61.1307)
- Haardt, F., & Maraschi, L. 1991, ApJL, 380, L51,
doi: [10.1086/186171](https://doi.org/10.1086/186171)
- Haardt, F., & Maraschi, L. 1993, ApJ, 413, 507,
doi: [10.1086/173020](https://doi.org/10.1086/173020)
- Honeycutt, R. K. 2001, PASP, 113, 473,
doi: [10.1086/319543](https://doi.org/10.1086/319543)
- Honeycutt, R. K., Cannizzo, J. K., & Robertson, J. W. 1994, ApJ, 425, 835, doi: [10.1086/174028](https://doi.org/10.1086/174028)
- Honeycutt, R. K., & Kafka, S. 2004, AJ, 128, 1279,
doi: [10.1086/422737](https://doi.org/10.1086/422737)
- Honeycutt, R. K., & Robertson, J. W. 1998, AJ, 116, 1961,
doi: [10.1086/300539](https://doi.org/10.1086/300539)
- Kara, E., Fabian, A. C., Cackett, E. M., Miniutti, G., & Uttley, P. 2013, MNRAS, 430, 1408,
doi: [10.1093/mnras/stt024](https://doi.org/10.1093/mnras/stt024)
- Kochanek, C. S., Shappee, B. J., Stanek, K. Z., et al. 2017, PASP, 129, 104502, doi: [10.1088/1538-3873/aa80d9](https://doi.org/10.1088/1538-3873/aa80d9)
- Kotov, O., Churazov, E., & Gilfanov, M. 2001, MNRAS, 327, 799, doi: [10.1046/j.1365-8711.2001.04769.x](https://doi.org/10.1046/j.1365-8711.2001.04769.x)
- Lasota, J.-P. 2001, NewAR, 45, 449,
doi: [10.1016/S1387-6473\(01\)00112-9](https://doi.org/10.1016/S1387-6473(01)00112-9)
- Linnell, A. P., Godon, P., Hubeny, I., et al. 2009, ApJ, 703, 1839, doi: [10.1088/0004-637X/703/2/1839](https://doi.org/10.1088/0004-637X/703/2/1839)
- Lyubarskii, Y. E. 1997, MNRAS, 292, 679
- Meyer, F., & Meyer-Hofmeister, E. 1981, A&A, 104, L10
- Meyer, F., & Meyer-Hofmeister, E. 1994, A&A, 288, 175
- Osaki, Y. 1974, PASJ, 26, 429
- Papadakis, I. E., & Lawrence, A. 1993, MNRAS, 261, 612,
doi: [10.1093/mnras/261.3.612](https://doi.org/10.1093/mnras/261.3.612)
- Ribeiro, F. M. A., & Diaz, M. P. 2007, AJ, 133, 2659,
doi: [10.1086/514335](https://doi.org/10.1086/514335)
- Ritter, H., & Kolb, U. 2003, A&A, 404, 301,
doi: [10.1051/0004-6361:20030330](https://doi.org/10.1051/0004-6361:20030330)
- Rodríguez-Gil, P., Schmidtobreick, L., & Gänsicke, B. T. 2007, MNRAS, 374, 1359,
doi: [10.1111/j.1365-2966.2006.11245.x](https://doi.org/10.1111/j.1365-2966.2006.11245.x)
- Scargle, J. D. 1982, ApJ, 263, 835, doi: [10.1086/160554](https://doi.org/10.1086/160554)
- Scaringi, S. 2014, MNRAS, 438, 1233,
doi: [10.1093/mnras/stt2270](https://doi.org/10.1093/mnras/stt2270)
- Scaringi, S., Kōrding, E., Uttley, P., et al. 2012, MNRAS, 427, 3396, doi: [10.1111/j.1365-2966.2012.22022.x](https://doi.org/10.1111/j.1365-2966.2012.22022.x)
- Schreiber, M. R., Hameury, J. M., & Lasota, J. P. 2003, A&A, 410, 239, doi: [10.1051/0004-6361:20031221](https://doi.org/10.1051/0004-6361:20031221)
- Shappee, B., Prieto, J., Stanek, K. Z., et al. 2014, in American Astronomical Society Meeting Abstracts, Vol. 223, American Astronomical Society Meeting Abstracts #223, 236.03
- Warner, B. 1995, Cambridge Astrophysics Series, 28
- Wilkins, D. R., Kara, E., Fabian, A. C., & Gallo, L. C. 2014, MNRAS, 443, 2746, doi: [10.1093/mnras/stu1273](https://doi.org/10.1093/mnras/stu1273)